

Phenomenological theory of the superconducting state inside the hidden-order phase of URu₂Si₂

Jian Kang and Rafael M. Fernandes

School of Physics and Astronomy, University of Minnesota, Minneapolis, MN 55455, USA

Recent experiments have unveiled important properties of the ground state of the elusive heavy fermion URu₂Si₂. While tetragonal symmetry-breaking was reported below the hidden-order (HO) transition at $T_{HO} \approx 17.5$ K, time-reversal symmetry-breaking was observed below the superconducting transition temperature $T_c < T_{HO}$. Although the latter results have been used to argue in favor of a chiral $d+id$ superconducting state, such an order parameter is incompatible with broken tetragonal symmetry. Here, we employ a phenomenological model to investigate the properties of a chiral superconducting state that develops inside the hidden-order phase. In this case, there are actually two superconducting transition temperatures: while T_c marks a normal-state to superconducting transition, $T_c^* < T_c$ signals a superconducting-to-superconducting transition in which time-reversal symmetry is broken. In the phase $T_c^* < T < T_c$, the low-energy density of states $\rho(\omega)$ is enhanced due to the crossing of two nodal lines, giving rise to an unusual $\omega \log(\omega)$ dependence of $\rho(\omega)$, which is manifested in several thermodynamic properties. We also investigate the emergence of a soft amplitude gap mode near T_c^* . In contrast to the usual amplitude mode near a regular normal-state to superconducting transition, this mode becomes soft near a superconducting-to-superconducting transition, which in principle allows for its detection by Raman spectroscopy. Finally, we investigate the impact of twin domains on the anisotropic properties of the superconducting state, and propose experiments in mechanically strained samples to explore the interplay between hidden order and superconductivity in URu₂Si₂.

I. INTRODUCTION

The nature of the ground state of the body-centered tetragonal compound URu₂Si₂ remains one of the most elusive problems in heavy fermion physics. At the HO transition temperature $T_{HO} \approx 17.5$ K, the system displays a sharp specific heat anomaly characteristic of a second-order phase transition¹⁻³. However, despite nearly thirty years of intense research, the broken symmetries of this hidden-order phase remain a widely debated topic. On the theory front, many different order parameters have been proposed to explain the hidden-order state, from high-rank multiple orders⁴⁻¹⁶ to exotic states involving the hybridization of localized and itinerant states¹⁷⁻³³. On the experimental front, recent measurements have provided important pieces for this long-standing puzzle. For instance, torque magnetometry^{34,35}, x-ray diffraction³⁶, and elasto-resistance measurements³⁷ have reported a tetragonal (C_4) to orthorhombic (C_2) transition simultaneously to T_{HO} , manifested by the inequivalence between the $[1\ 1\ 0]$ and $[1\ -1\ 0]$ directions of the crystallographic unit cell (see Fig. 1). Whether this is the only broken symmetry in the hidden-order state – in which case it would be classified as a nematic state – remains an open issue^{38,39}. For instance, quantum oscillation measurements also suggest a translational symmetry-breaking along the c -axis⁴⁰, and neutron elastic scattering experiments favor a rank 5 multipole order in the system⁴¹.

In comparison to the hidden-order phase, the superconducting state of URu₂Si₂ that appears at $T_c \approx 1.5$ K has received rather less attention. Understanding its nature is relevant not only within the bigger picture of su-

perconductivity in heavy-fermion compounds, but also as a potential tool to probe the properties of the HO state^{42,43}, since superconductivity develops well below T_{HO} and disappears when the HO phase is suppressed by external pressure^{44,45}. An interesting proposal based on recent angle-resolved specific heat⁴⁶ and thermal conductivity data⁴⁷, which reported indirect evidence for point and line nodes, is of a chiral d -wave superconducting (SC) state described by the order parameter⁴⁷:

$$\Delta(k) = \Delta_0 \sin \frac{k_z}{2} \left(\sin \frac{k_x + k_y}{2} \pm i \sin \frac{k_x - k_y}{2} \right). \quad (1)$$

Such a SC state breaks time-reversal symmetry, which seems to be in agreement with magnetic susceptibility⁴⁸ and recent Kerr effect measurements⁴⁹. However, this order parameter manifestly preserves C_4 symmetry, whereas the HO state, from which SC develops, breaks tetragonal symmetry.

In this paper, we use a phenomenological model to reconcile the proposal of a chiral d -wave state with the experimental observations of a HO state that breaks C_4 symmetry. While a phenomenological approach leaves aside the issue of the microscopic mechanisms involved in the formation of these phases, it allows for general conclusions to be drawn regardless of one's favorite order parameter for the HO phase – as long as it accounts for C_4 symmetry breaking. As a result, it provides general benchmarks that must be satisfied if indeed the HO state breaks C_4 symmetry and the SC state is chiral. One obvious consequence from the fact that SC develops in a C_2 background, as pointed out in different scenarios⁵⁰⁻⁵², is that the chiral superconducting transition is actually split into two superconducting transitions T_c and T_c^* .

While at T_c the system first becomes superconducting, at $T_c^* < T_c$ time-reversal symmetry (TRS) is broken, signaling a SC-SC transition. Our focus in this paper is on the thermodynamic properties of these two distinct superconducting phases. We find that, while in the regime $T < T_c^*$ the nodal quasi-particle density of states $\rho(\omega)$ depends linearly on ω for low-energies, reflecting the presence of point and line nodes, in the regime $T_c^* < T < T_c$ the density of states acquires an unusual log-dependence $\rho(\omega) \sim \omega \log \omega$ due to the crossing between two nodal lines. Such a behavior leaves signatures in several thermodynamic quantities, such as the specific heat and the penetration depth.

Furthermore, we investigate how the anisotropies of the SC state in both regimes – namely $T < T_c^*$ and $T_c^* < T < T_c$ – are affected by the presence of twin domains with different C_2 orientational order. By calculating the angular dependence of the specific heat in the presence of a magnetic field, we find that a twinned sample and a sample with no C_4 broken symmetry would display nearly identical behaviors. This helps to reconcile some of the experimental results that led to the proposal of a chiral SC state, as in Eq. (1), with the experimental results that found tetragonal symmetry-breaking in the HO phase. We propose experiments in mechanically detwinned samples to unveil the intrinsic anisotropies of the SC state.

We also find an unusual behavior for the collective SC modes near T_c^* . In a common normal-state to SC transition, the soft amplitude SC gap-mode falls into the continuum and is strongly damped. However, because T_c^* is a SC-SC transition, the corresponding soft amplitude mode develops in the background of a superconducting quasi-particle spectrum. Despite the presence of nodal quasi-particles in this spectrum, which promote under-damping of the soft amplitude mode, we argue that this collective mode may still be observed in the excitation spectrum, as measured by Raman scattering.

The paper is organized as follows: in Section II we present our phenomenological model for the SC state inside the HO phase and discuss its nodal quasi-particle spectrum for different temperature regimes. In Section III we study the impact of twin domains on the anisotropic thermodynamic properties of the SC state, with particular emphasis on the angle-dependent specific heat. Section IV is devoted to the investigation of the collective modes of the SC state. Concluding remarks follow in Section V.

II. PHENOMENOLOGICAL MODEL

A. Superconducting free energy

The SC order parameter in Eq. (1) belongs to the E_g irreducible representation of the tetragonal point group. Its degeneracy stems from the two-dimensionality of the E_g representation. However, because the HO state

breaks the C_4 symmetry, the SC order parameter must be modified to reflect the new orthorhombic point group symmetry of the system. Using as a starting point Eq. (1), we can describe the chiral d -wave SC order parameter inside the orthorhombic HO phase as a two-component order parameter:

$$\Delta(k) = \Delta_1 \sin \frac{k_z}{2} \sin \frac{k_x + k_y}{2} + e^{i\theta} \Delta_2 \sin \frac{k_z}{2} \sin \frac{k_x - k_y}{2}, \quad (2)$$

where θ is the phase difference between the two components of the order parameter, and Δ_i are real order parameters. TRS is kept intact only if $\theta = 0, \pi$. The absolute value of the gap function is then:

$$|\Delta|^2 = \sin^2 \frac{k_z}{2} \left[\Delta_1^2 \sin^2 \frac{k_x + k_y}{2} + \Delta_2^2 \sin^2 \frac{k_x - k_y}{2} + 2\Delta_1 \Delta_2 \cos \theta \sin \frac{k_x + k_y}{2} \sin \frac{k_x - k_y}{2} \right] \quad (3)$$

Thus, tetragonal symmetry requires $\theta = \pm\pi/2$ and $\Delta_1 = \Delta_2$, but in the HO phase this is not the case.

To proceed, we need to establish how the tetragonal symmetry is broken in the hidden order phase. There are two possibilities: either the horizontal $[1\ 0\ 0]$ and vertical $[0\ 1\ 0]$ directions become inequivalent, in which case the C_2 order parameter belongs to the B_{1g} irreducible representation, or the diagonal $[1\ 1\ 0]$ and anti-diagonal $[1\ -1\ 0]$ directions become inequivalent, in which case the C_2 order parameter belongs to the B_{2g} irreducible representation. Torque magnetometry³⁵, x-ray diffraction³⁶, and elasto-resistance measurements³⁷ all agree on the second scenario, which is schematically shown in Fig. 1.

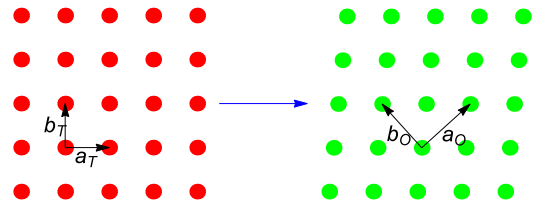


Figure 1. The basal plane across the HO phase transition. Left: above the HO phase, the crystal structure (here centered at the U atoms) is body centered tetragonal. Right: The HO phase breaks the fourfold rotational symmetry on the ab plane by making the $[1\ 1\ 0]$ and $[1\ -1\ 0]$ directions (parallel to the Ru nearest neighbor directions) inequivalent. The crystal structure becomes base centered orthorhombic.

Thus, we can now write down the phenomenological Ginzburg-Landau model for the superconducting degrees

of freedom inside the HO phase⁵³:

$$F_{\text{SC}} = \frac{a}{2} (\Delta_1^2 + \Delta_2^2) + \frac{u}{4} (\Delta_1^4 + \Delta_2^4) + \frac{1}{2} \Delta_1^2 \Delta_2^2 (\beta + \alpha \cos 2\theta) - \frac{\eta}{2} (\Delta_1^2 - \Delta_2^2), \quad (4)$$

Here, $a = a_0 (T - T_{c,0})$ and the order parameter $\eta \neq 0$ describes the C_4 symmetry-breaking inside the HO state. We refrain from calling it the HO order parameter, since it is unclear whether other symmetries are also broken in the HO phase. In any case, because $T_{\text{HO}} \gg T_c$, we consider η to be constant on the temperature regime in which an expansion in powers of the superconducting order parameter is allowed. Without loss of generality, we assume in this section that $\eta > 0$ – in the next section, where we consider the effects of domains, this assumption is no longer valid.

For the SC state to be a chiral d -wave, α must be positive; furthermore, in order for both order parameter components to coexist, and for the free energy to be bounded, we must also have $u > |\beta - \alpha|$. With this constraints, minimization of the free energy with respect to θ gives always $\theta = \pm\pi/2$, as long as both Δ_1 and Δ_2 are simultaneously non-zero.

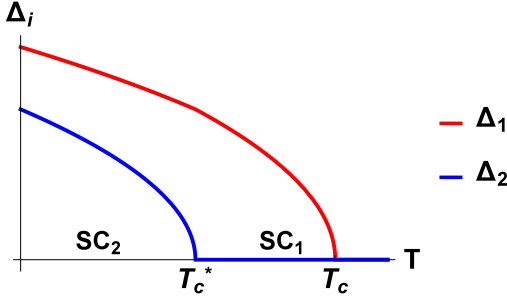


Figure 2. The SC order parameters in different phases. Δ_1 becomes nonzero when $T < T_c$ (SC₁ phase), and Δ_2 becomes nonzero at $T < T_c^*$ (SC₂ phase). The system, therefore, has two different SC phases. The phase difference between Δ_1 and Δ_2 is $\pi/2$, i.e. time reversal symmetry is broken only in the SC₂ phase.

Minimization of the free energy with respect to Δ_1 and Δ_2 reveal two distinct regimes as shown in Fig 2, defined by the two transition temperatures:

$$\begin{aligned} T_c &= T_{c,0} + \frac{\eta}{a_0} \\ T_c^* &= T_c - \frac{2u\eta}{a_0(u - \beta + \alpha)} \end{aligned} \quad (5)$$

Here, we assume that $a = a_0(T - T_{c,0})$ when the temperature is close to $T_{c,0}$. For $T_c^* < T < T_c$ (SC₁ phase), the free energy is minimized by enforcing only one of the SC components to be non-zero:

$$\begin{aligned} \Delta_1^2 &= -\left(\frac{a - \eta}{u}\right); & \Delta_2 &= 0 \\ F_{\text{min}} &= -\frac{(a - \eta)^2}{4u}. \end{aligned} \quad (6)$$

On the other hand, for $T < T_c^*$ (SC₂ phase), the minimum of the free energy corresponds to the condensation of the two components with a $\pi/2$ phase difference:

$$\begin{aligned} \theta &= \pi/2, \\ \Delta_1^2 &= -\frac{a}{u + \beta - \alpha} + \frac{\eta}{u - \beta + \alpha}, \\ \Delta_2^2 &= -\frac{a}{u + \beta - \alpha} - \frac{\eta}{u - \beta + \alpha}, \\ F_{\text{min}} &= -\frac{a^2}{2(u + \beta - \alpha)} - \frac{\eta^2}{2(u - \beta + \alpha)}. \end{aligned} \quad (7)$$

Because the free energy changes smoothly, both transitions are second-order. At T_c , the system becomes a single-component SC, whereas at T_c^* , TRS is broken, and the system becomes a two-component SC. The anisotropy induced in Δ_1 and Δ_2 is proportional to η , as expected, since this order parameter manifestly breaks the tetragonal symmetry. The splitting between T_c and T_c^* is also proportional to $|\eta|$.

It is important to discuss the relationship between the orthorhombic distortion δ in the C_2 HO phase and the electronic anisotropy order parameter η introduced here. Symmetry arguments enforce them to be proportional to each other, i.e. $\langle \delta \rangle \propto \langle \eta \rangle$. However, the fact that δ is small in the HO phase ($\delta \sim 10^{-5}$ as measured by x-ray diffraction³⁶) does not imply that η is also necessarily small. If indeed the anisotropy is electronically driven, as suggested by the elasto-resistance measurements³⁷, one would expect η to be sizable even if δ is small. This is the case, for instance, in optimally-doped iron-based superconductors, where the in-plane resistivity anisotropy is $\rho_b/\rho_a \sim 1.5$ even though $\delta \sim 10^{-4}$ (for reviews, see^{54,55}).

B. Nodal quasi-particle density of states

Having established the existence of two SC states in URu₂Si₂, we now discuss their thermodynamic properties. At low temperatures, they are determined by the low-energy properties of the quasi-particle density of states (DOS) $\rho(\omega)$. For instance, the specific heat C , the penetration depth λ_p , and the spin-lattice relaxation rate $1/T_1T$ are given by:

$$\begin{aligned} \frac{C}{T} &\propto \int d\omega \rho(\omega) (\beta\omega)^2 \left(-\frac{\partial f}{\partial \omega}\right) \\ \lambda_p^{-2} - \lambda_{p,0}^{-2} &\propto \int d\omega \rho(\omega) \left(-\frac{\partial f}{\partial \omega}\right) \\ (T_1T)^{-1} &\propto \int d\omega \rho^2(\omega) \left(-\frac{\partial f}{\partial \omega}\right) \end{aligned} \quad (8)$$

At low energies, the DOS is determined by the dispersion of the nodal quasi-particles. The latter are remarkably different for the two SC states. For the higher-temperature SC state at $T_c^* < T < T_c$, which we denote SC₁, only one of the gap components is condensed and the gap function contains horizontal zeros at $k_z = 0, \pm 2\pi$ and vertical zeros at $k_x = -k_y$ (if $\Delta_1 \neq 0$) or at $k_x = k_y$ (if $\Delta_2 \neq 0$). On the other hand, for the lower-temperature SC state at $T < T_c^*$, which we denote SC₂, the gap vanishes along the plane $k_z = 0, \pm 2\pi$ and along the line $k_x = k_y = 0$.

To proceed, we need to establish whether these gap zeros cross the Fermi surface, forming nodal quasi-particles. The Fermi surface of URu₂Si₂ is remarkably complex: first-principle calculations in the paramagnetic phase show the existence of hole-like ellipsoids centered at $\Gamma = (0, 0, 0)$ and $Z = (0, 0, 2\pi)$, and electron-like ellipsoids centered at $M = (\pi, \pi, 0)$ ^{27,56}. Although it is unclear how the hybridization with the 5*f* U states affects this Fermi surface configuration, or whether there is an additional folding of the band structure along the $(0, 0, 2\pi)$ momentum, as in the magnetically ordered phase, quantum oscillation measurements^{40,57–60} seem to be consistent with at least one pocket centered at Γ . For the purposes of determining the low-energy properties of the DOS, we therefore consider a single spherical pocket centered at Γ . In this case, in the SC₁ state, there are two crossing nodal lines at $k_{F,z} = 0$ and $k_{F,x} = \pm k_{F,y}$. In the SC₂ phase, there remains a nodal line at $k_{F,z} = 0$ and a couple of nodal points at $k_{F,x} = k_{F,y} = 0$. Both nodal configurations are shown in Fig. 3.

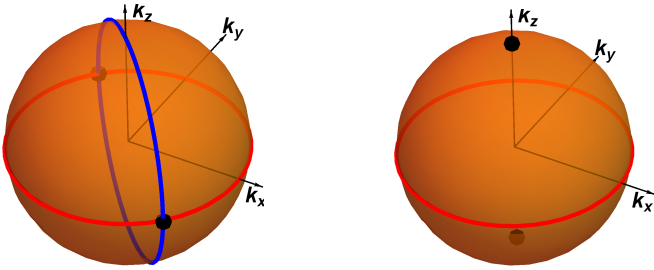


Figure 3. Nodes on a Fermi surface centered at Γ in the two different SC phases. Left: In the SC₁ phase, the Fermi surface contains the horizontal nodal line $k_z = 0$ (red curve) and the vertical nodal line $k_x + k_y = 0$ (blue curve). Right: in the SC₂ phase, the Fermi surface contains only one horizontal nodal line $k_z = 0$ (red curve) and two nodal points $(0, 0, \pm k_F)$ (black dots).

We first consider the higher-temperature SC₁ state ($T_c^* < T < T_c$). For concreteness, we assume $\Delta_1 \neq 0$ and $\Delta_2 = 0$, but the results are the same for the con-

verse. The DOS is given by:

$$\begin{aligned} \rho(\omega > 0) &= \frac{1}{V} \sum_{\vec{k}} \delta(\omega - E(\vec{k})) \\ &= N_0 \int \frac{d\Omega_{\hat{k}}}{4\pi} \int d\xi \delta(\omega - \sqrt{\xi^2 + \Delta^2(\hat{k})}) \\ &= N_0 \omega \int \frac{d\Omega_{\hat{k}}}{4\pi} \text{Re} \frac{1}{\sqrt{\omega^2 - \Delta^2(\hat{k})}}, \end{aligned} \quad (9)$$

where N_0 is the DOS at the Fermi level, and $\Delta(\hat{k})$ is the SC gap along the Fermi pocket centered at Γ . The latter can be conveniently described in terms of the polar and azimuthal angles θ and ϕ around the spherical pocket:

$$\begin{aligned} \Delta(\hat{k}) &= \Delta_1 \sin \frac{k_z}{2} \sin \frac{k_x + k_y}{2} \\ &\approx \Delta_1 \sin 2\theta \cos \left(\phi - \frac{\pi}{4} \right), \end{aligned} \quad (10)$$

where Δ_1 has been rescaled by the factor $\Delta_1 \rightarrow \Delta_1 \sqrt{2} (k_F a)^2 / 8$. There are two nodal lines at $\theta_0 = \pi/2$ ($k_z = 0$) and $\phi_0 = -\pi/4, 3\pi/4$ ($k_x = -k_y$), which intersect along the Fermi surface at a single point, giving rise to a quadratic node. Expanding the DOS for small energies $\omega \ll \Delta_1$, we find the asymptotic behavior:

$$\rho(\omega) \approx N_0 \left(\frac{\omega}{2\Delta_1} \log \frac{\Delta_1}{\omega} + \frac{\omega}{\Delta_1} \log 4 \right) \quad (11)$$

Fig. 4 compares the numerically-evaluated DOS with the asymptotic expression (11) as function of energy, evidencing the dominant $\omega \log \omega$ behavior at low energies.

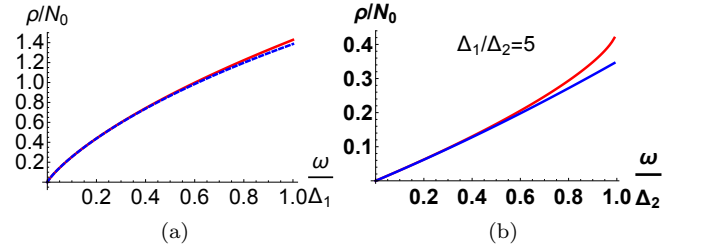


Figure 4. The low energy DOS computed numerically (red curve) and via its asymptotic expression (blue curve). Left: DOS in the high-temperature SC₁ phase ($T_c^* < T < T_c$). The blue curve is the asymptotic expression (11) with the dominant $\omega \log \omega$ behavior at low energies. Right: DOS in the low-temperature SC₂ phase ($T < T_c^*$). The blue curve is the asymptotic expression (15) with the dominant ω behavior at low energies.

A careful analysis of Eq. (11) reveals that while the linear-in- ω term arises from the contribution of each individual nodal line, the $\omega \log \omega$ term arises from the crossing point between the two nodal lines. To make this transparent, we expand the SC order parameter in the vicinity of one of the two crossing points, $\theta_0 = \pi/2$, $\phi_0 = 3\pi/4$:

$$\Delta(\theta, \phi) = 2\Delta_1 (\theta - \theta_0) (\phi - \phi_0). \quad (12)$$

Clearly, the nodal dispersion is quadratic rather than linear^{61–64}. Substituting this expression in Eq. (9) and restricting the integration to the proximities of the crossing point, $|\theta - \theta_0|, |\phi - \phi_0| < \Lambda$, yields:

$$\rho(\omega) \approx 4N_0 \frac{\omega}{2\Delta_1} \int_0^\Lambda d\tilde{\theta} \int_0^\Lambda d\tilde{\phi} \operatorname{Re} \frac{1}{\sqrt{\left(\frac{\omega}{2\Delta_1}\right)^2 - \tilde{\phi}^2 \tilde{\theta}^2}}, \quad (13)$$

where $\tilde{\theta} = \theta - \theta_0$, $\tilde{\phi} = \phi - \phi_0$. A straightforward calculation gives:

$$\rho(\omega) \approx \pi N_0 \frac{\omega}{\Delta_1} \log \left(\frac{4\Lambda^2 \Delta_1}{\omega} \right). \quad (14)$$

Clearly, the additional logarithmic contribution is a consequence of the quadratic dispersion near the crossing point of two nodal lines. Note that it will also give rise to logarithmic corrections to the low-temperature behavior of the thermodynamic quantities listed in the beginning of this section. More generally, tunneling experiments sensitive to $\rho(\omega)$ may in principle be able to identify this additional logarithmic contribution, which would be unambiguous evidence for this type of superconducting gap function.

In the low-temperature SC₂ phase at $T < T_c^*$, $\Delta_2 \neq 0$ and one of the nodal lines is replaced by two nodal points. As a result, the logarithmic corrections discussed above disappear. Indeed, the system in the SC₂ phase contains only one nodal line $k_z = 0$, and two nodal points $k_x = k_y = 0$. Computing the DOS at low energies, $\omega \ll \Delta_2, \Delta_1$, we find:

$$\rho(\omega) \approx N_0 \left[\frac{\omega}{2\Delta_1} \ln \left(\frac{4\Delta_1}{\Delta_2} \right) + \frac{\omega^2}{4\Delta_1 \Delta_2} \right] \quad (15)$$

As expected, the nodal line gives a linear contribution to the DOS, whereas the nodal points give a quadratic contribution. Of course, at energies higher than the scale of Δ_2 , but still much smaller than Δ_1 , there is a crossover to the logarithmic behavior found in the SC₁ phase, which may be detectable experimentally.

Interestingly, the coefficient of the linear-in- ω term depends on the ratio Δ_1/Δ_2 , which in turn depends on the C_4 symmetry-breaking parameter η , according to Eq. (7). The dependence of this linear coefficient on η is shown in Fig. 5 below. This result reveals an interesting possibility to probe the impact of the tetragonal symmetry breaking of the HO phase on the SC properties. Specifically, one could experimentally extract this linear coefficient – either from tunneling experiments or from penetration depth data – and study its dependence on compressive and tensile external strain, which would tend to increase or reduce the value of η .

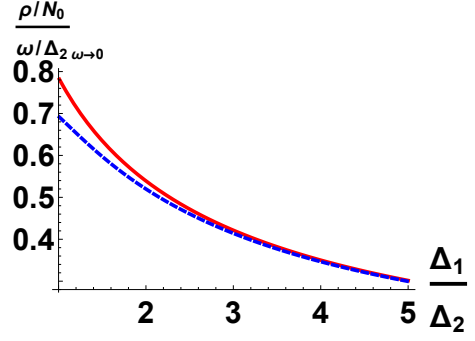


Figure 5. The linear coefficient of ω in the low energy DOS of the SC₂ phase as function of $\frac{\Delta_1}{\Delta_2} - 1 \propto \eta$. The red curve is the numerical result and the blue curve corresponds to the asymptotic expression (15).

III. ANISOTROPIC PROPERTIES OF THE SUPERCONDUCTING STATE

Having established the thermodynamic properties of the SC₁ and SC₂ phases, we now discuss how the in-plane anisotropy appearing at the HO transition temperature is manifested in the superconducting properties. From symmetry considerations, one expects anisotropies in the in-plane penetration depth, critical magnetic field H_{c2} , etc. Experimentally, the behavior of the specific heat as function of the angle of an external magnetic field \vec{H} has been used as a probe of the nodal structure of the superconducting gap in URu₂Si₂⁴⁶. Thus, given the experimental feasibility and the existence of current data, we focus here on the magnetic-field angle-dependent specific heat, $C(\vec{H})$, in both SC₁ and SC₂ phases. In the presence of an external magnetic field, a nodal superconductor acquires a finite density of states $\rho(\vec{H})$ at $T = 0$. As a result, the specific heat at low temperatures is given by $C(\vec{H})/T \propto \rho(\vec{H})$. In a tetragonal system, $\rho(\vec{H})$ displays four-fold oscillations as the azimuthal angle of the applied magnetic field \vec{H} changes. However, in an orthorhombic system, which is the case of URu₂Si₂ below the HO transition, two-fold oscillations are expected.

A complete description of $\rho(\vec{H})$, which is beyond the scope of this work, requires detailed knowledge of the Fermi surface and of the microscopic mechanisms of the superconducting state^{65,66}. Here, we are interested in contrasting the anisotropies introduced by η and manifested in $\rho(\vec{H})$ in both SC phases, and also in studying the impact of twin domains present in real materials. Therefore, to keep the discussion general and meaningful, we consider a spherical Fermi surface and the semi-classical approximation for $\rho(\vec{H})$ first introduced by Volovik⁵¹. Valid in the regime of low fields and low temperatures, where the vortex lattice of the mixed state is dilute, this approximation focuses on the contributions of the extended quasi-particles around a single vortex, neglecting the contribution from the vortex core states. The main effect arises from the supercurrent $\vec{v}_s(\vec{r})$ gener-

ated by an isolated vortex, which causes a Doppler shift $\Delta E = \vec{k} \cdot \vec{v}_s(\vec{r})$ in the quasi-particle excitation spectrum. Taking the spatial average over the unit cell of the vortex lattice then gives the zero-energy DOS^{51,65}:

$$\rho(\vec{H}) = \frac{1}{V} \sum_{\vec{k}} \int \frac{d^2 r}{A} \delta(\vec{k} \cdot \vec{v}_s - E_{\vec{k}}) \quad (16)$$

where $A = \Phi_0/H = \pi R^2$ is the area of the vortex lattice unit cell, which in turn is approximated by a circle of radius $R = \sqrt{\Phi_0/(\pi H)}$. Here, Φ_0 is the flux quantum and $E_{\vec{k}} = \sqrt{\xi_{\vec{k}}^2 + \Delta^2(\vec{k})}$ is the quasi-particle energy. For an arbitrary magnetic field along the \hat{n} direction, $\vec{H} = H\hat{n}$, the supercurrent velocity \vec{v}_s is given by:

$$\vec{v}_s = \frac{1}{2mr} \hat{n} \times \hat{r}. \quad (17)$$

To proceed, it is convenient to define the angle-dependent Doppler-shift energy:

$$E_D(\vec{k}) = \frac{k_f}{2mR} |\hat{n} \times \hat{k}|, \quad (18)$$

Evaluation of the DOS in Eq. (16) then gives:

$$\frac{\rho(\vec{H})}{N_0} = \int \frac{d\Omega_{\hat{k}}}{4\pi} \begin{cases} \frac{E_D^2(\hat{k})}{\Delta^2(\hat{k})} & \text{if } E_D(\hat{k}) \leq |\Delta(\hat{k})| \\ 1 & \text{if } E_D(\hat{k}) \geq |\Delta(\hat{k})| \end{cases} \quad (19)$$

It is convenient to define the ratio between the Doppler-shift energy scale and the magnitude of the SC gap:

$$\gamma = \frac{k_F}{4mR\Delta_1}, \quad (20)$$

We consider first the SC₁ state, when $\Delta_1 \neq 0$ and $\Delta_2 = 0$. Since we are interested mainly on the in-plane anisotropies promoted by the HO tetragonal symmetry-breaking parameter η , hereafter we consider the situation in which \vec{H} is swept across the ab plane, and therefore characterized by the azimuthal angle ϕ_h . Using the expansion (10) for Δ_1 yields the expression:

$$\frac{E_D(\hat{k})}{2|\Delta(\hat{k})|} = \gamma \frac{\sqrt{1 - \sin^2 \theta \cos^2(\phi - \phi_h)}}{|\sin 2\theta \cos(\phi - \frac{\pi}{4})|} \quad (21)$$

which can be substituted in Eq. (19) for numerical evaluation. In the weak field limit, $\gamma \ll 1$, we obtain the analytical expression:

$$\frac{\rho(\phi_h)}{4N_0} \approx \gamma + \left| \cos\left(\phi_h - \frac{\pi}{4}\right) \right| \gamma \left(\frac{1}{\pi} \ln \frac{2}{\gamma} - 1 \right) \quad (22)$$

This formula captures the general behavior of the numerically-calculated $\rho(\phi_h)$, plotted in Fig. 6. In particular, it reveals a clear in-plane two-fold anisotropy of $\rho(\phi_h)$, with a maximum at $\phi_h = \pi/4, -3\pi/4$ and a minimum at $\phi_h = -\pi/4, 3\pi/4$. This behavior is a consequence of the quadratic node present in the Fermi surface at $\phi_0 = \pi/4, \theta_0 = \pi/2$ (see the previous Section): when \vec{H} is parallel to the quadratic node momentum, the Doppler shift in the nodal quasi-particle spectrum is maximum, but when \vec{H} is perpendicular to the quadratic node momentum, the Doppler shift is minimum.

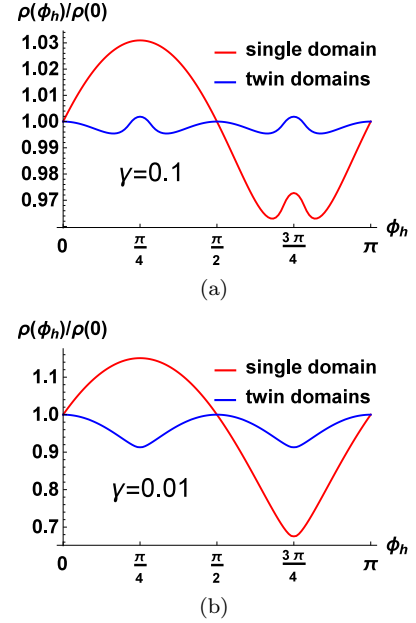


Figure 6. The angle-dependent DOS in the presence of an in-plane magnetic field in the SC₁ state. The ratio between the Doppler shift energy and the gap is set to $\gamma = 0.1$ in panel (a) and $\gamma = 0.01$ in panel (b). ϕ_h is the azimuthal angle of the magnetic field. The red curve corresponds to a single domain with $\Delta_2 = 0$, whereas the blue curve corresponds to a twin domain with equal-weight $\Delta_2 \neq 0, \Delta_1 = 0$ and $\Delta_1 \neq 0, \Delta_2 = 0$.

We now consider the SC₂ phase, which is the most relevant for comparison with experiments, since the latter are commonly performed at very low temperatures – presumably below both T_c and T_c^* . In the SC₂ phase, both Δ_1 and Δ_2 are non-zero, but non-equal. We obtain:

$$\frac{E_D(\hat{k})}{2|\Delta(\hat{k})|} = \gamma \frac{\sqrt{1 - \sin^2 \theta \cos^2(\phi - \phi_h)}}{|\sin 2\theta| \sqrt{\cos^2(\phi - \frac{\pi}{4}) + \frac{\Delta_2^2}{\Delta_1^2} \sin^2(\phi - \frac{\pi}{4})}} \quad (23)$$

which can then be substituted in Eq. (19) to compute the DOS. In Fig. 7, we plot $\rho(\phi_h)$ for two different values of the parameter γ , considering the ratio $\Delta_1/\Delta_2 = 2$. The behavior is similar to the SC₁ phase, namely, the DOS is two-fold anisotropic and maximum at $\phi_h = \pi/4, -3\pi/4$

but minimum at $\phi_h = -\pi/4, 3\pi/4$. The contrast between the maximum and the minimum is proportional to the ratio Δ_1/Δ_2 . In the C_4 symmetric case, $\Delta_1 = \Delta_2$, to leading order in γ , $\rho(\phi_h)$ is angle-independent and constant, $\rho(\phi_h) = 4\gamma/\pi + \gamma^2 \ln(2/\gamma)$.

An important issue is whether the two-fold anisotropy induced by the difference between Δ_1 and Δ_2 (which in turn arises from the HO C_4 symmetry-breaking term η) can be observed experimentally. In our analysis, so far we have considered only the ideal scenario in which a single C_2 domain is formed. In large samples – at least large enough to allow one to measure the specific heat – it is very likely that the system will break up in twin domains with $\eta > 0$ (corresponding to $\Delta_2 = 0$ in the SC_1 phase and $\Delta_1 > \Delta_2$ in the SC_2 phase) and $\eta < 0$ (corresponding to $\Delta_1 = 0$ in the SC_1 phase and $\Delta_1 < \Delta_2$ in the SC_2 phase). As a result, the two-fold anisotropy is washed out. To capture this effect, we calculated $\rho_t(\phi_h)$ of a twin-domain system:

$$\rho_t(\phi_h) = \frac{1}{2}\rho(\phi_h) + \frac{1}{2}\rho(\phi_h + \pi/2). \quad (24)$$

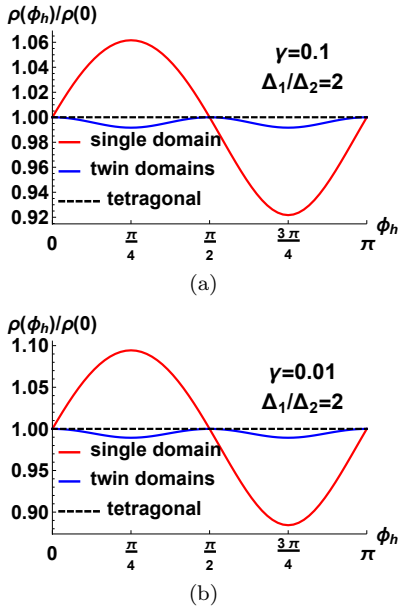


Figure 7. The angle-dependent DOS in the presence of an in-plane magnetic field in the SC_2 state ($\Delta_1, \Delta_2 \neq 0$). The ratio between the Doppler shift energy and the gap is set to $\gamma = 0.1$ in the upper panel and $\gamma = 0.01$ in the lower panel. ϕ_h is the azimuthal angle of the magnetic field. The red curve corresponds to a single domain with $\Delta_1/\Delta_2 = 2$, whereas the blue curve corresponds to a twin domain with equal-weight $\Delta_1/\Delta_2 = 2$ and $\Delta_1/\Delta_2 = 1/2$. The dashed black curve corresponds to the tetragonal symmetric system, with $\Delta_1 = \Delta_2$.

The results for both SC_1 and SC_2 phases in the twin-domain case are shown by the blue curves in Figs. 6 and 7. While for the SC_1 phase there is a small four-fold anisotropy reminiscent of the anisotropies of the

single-domain case, in the SC_2 phase the DOS is basically angle-independent and indistinguishable from the tetragonal case ($\Delta_1 = \Delta_2$). Interestingly, the in-plane angle-resolved specific heat data reported in⁴⁶ is nearly flat as the field is swept from the a axis to the b axis.

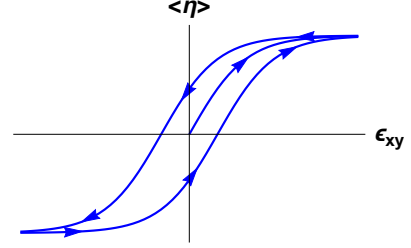


Figure 8. Bulk averaged anisotropy $\langle \eta \rangle$ as function of the in-plane uniaxial strain ϵ_{xy} . Without uniaxial strain, $\langle \eta \rangle = 0$ as averaged over different domains. It becomes nonzero upon application of uniaxial strain and remains non-zero even after the strain is released, inside the symmetry-broken phase.

In order to decide whether the experimentally observed behavior is compatible with the orthorhombic SC_2 phase or with the tetragonal SC chiral phase, we propose to perform angle-resolved specific heat experiments in samples under uniaxial external strain. In both cases, applying either compressive or tensile stress along the a (or b) axis will induce a two-fold anisotropy in $\rho(\phi_h)$ – similarly to what we calculated for a single-domain case. This is not surprising, as the external strain explicitly breaks the C_4 symmetry – in other words, it generates itself a term η in the free energy (4) regardless of whether the symmetry was spontaneously broken at the HO transition. However, upon releasing the strain, only in the SC_2 phase a non-zero η remains due to the alignment of the twin domains: This is nothing but the manifestation of the hysteresis associated with the symmetry-broken phase (see Fig. 8). Therefore, if the two-fold anisotropies of $\rho(\phi_h)$ persist after the applied strain is released, this would be unambiguous proof of the anisotropy in Δ_1 and Δ_2 characteristic of the SC_2 phase. Note that devices capable of applying and releasing strain in a controlled way have been now widely used to study the nematic phase of the iron-based superconductors⁶⁷.

IV. COLLECTIVE MODES IN THE SUPERCONDUCTING PHASE

As discussed above, inside the HO phase there are two SC transitions: at T_c , the system undergoes a normal-state to SC transition, characterized by the condensation of one of the two components of the chiral SC order parameter (Δ_1 if $\eta > 0$). At $T_c^* < T_c$, a SC-to-SC transition takes place, in which the second component of the SC order parameter condenses (Δ_2 if $\eta > 0$) with a $\pi/2$ relative phase with respect to the other component, breaking time-reversal symmetry. Detection of the sec-

and SC transition in URu₂Si₂ would be strong evidence for the scenario discussed here. Besides the usual thermodynamic signatures of a SC transition, for instance in the specific heat, the system also displays distinctive collective SC excitations at T_c^* – which in turn could be measured by spectroscopic techniques such as Raman scattering.

To understand why this is the case, we note that the collective modes of a single-band superconductor are the phase and amplitude (also called Higgs) modes. While the former is always gapped by the Anderson-Higgs mechanism, the latter becomes soft near the superconducting transition. Near the usual normal-state to SC transition (such as the one taking place at T_c in our system), the energy gap of the amplitude mode is generally larger than the SC gap, implying that the mode decays into the particle-hole continuum. However, near a SC-to-SC transition (such as the one taking place at T_c^* in our system) the situation is different, because the electronic spectrum has already been gapped by the first SC transition. As a result, it becomes in principle possible to obtain a sharp SC amplitude mode at T_c^* that does not fall into the particle-hole continuum^{68–71}. The situation is similar to the appearance of the so-called Bardasis-Schrieffer mode in superconductors with nearly-degenerate superconducting states⁷².

To investigate this scenario, we include the time-dependence of the SC order parameter in the free energy

(4):

$$\tilde{F}_{\text{SC}} \left(\Delta_i, \frac{\partial \Delta_i}{\partial t} \right) = \sum_{i=1}^2 \gamma_{\text{sc}} \left| \frac{\partial \Delta_i}{\partial t} \right|^2 - F_{\text{SC}}(\Delta_i) , \quad (25)$$

where F_{SC} is given by Eq. (4) and the coefficient of the time-dependent term is $\gamma_{\text{sc}} > 0$. Because we are interested in the behavior below T_c , where the SC system is particle-hole symmetric, the time-dependent term must be quadratic in the time-derivative, in contrast to the usual linear $i\Delta^* \frac{\partial \Delta}{\partial t}$ term that appears in the Gross-Pitaevskii equation, where particle-hole symmetry is not necessarily present^{68,73}.

To calculate the collective modes of the system, we linearize the gap equations near T_c by writing $\Delta_i = \Delta_{i,0} + \delta \Delta_i$, where $\Delta_{i,0}$ are the solutions of the time-independent equations, i.e. $\left(\frac{\partial F_{\text{SC}}}{\partial \Delta_i} \right)_{\Delta_{i,0}} = 0$. We obtain the coupled linear equations:

$$-\gamma_{\text{sc}} \frac{\partial^2}{\partial t^2} \begin{pmatrix} \delta \Delta_1 \\ \delta \Delta_1^* \\ \delta \Delta_2 \\ \delta \Delta_2^* \end{pmatrix} = \mathbf{\Lambda}(\Delta_{i,0}) \begin{pmatrix} \delta \Delta_1 \\ \delta \Delta_1^* \\ \delta \Delta_2 \\ \delta \Delta_2^* \end{pmatrix} \quad (26)$$

with the matrix:

$$\mathbf{\Lambda}(\Delta_i) = \begin{pmatrix} \frac{a-\eta}{2} + u|\Delta_1|^2 + \frac{\beta}{2}|\Delta_2|^2 & \frac{u}{2}\Delta_1^2 + \frac{\alpha}{2}\Delta_2^2 & \frac{\beta}{2}\Delta_1\Delta_2^* + \alpha\Delta_1^*\Delta_2 & \frac{\beta}{2}\Delta_1\Delta_2 \\ \frac{u}{2}\Delta_1^2 + \frac{\alpha}{2}\Delta_2^2 & \frac{a-\eta}{2} + u|\Delta_1|^2 + \frac{\beta}{2}|\Delta_2|^2 & \frac{\beta}{2}\Delta_1^*\Delta_2^* & \frac{\beta}{2}\Delta_1^*\Delta_2 \\ \frac{\beta}{2}\Delta_1\Delta_2^* + \alpha\Delta_1\Delta_2^* & \frac{\beta}{2}\Delta_1\Delta_2 & \frac{a+\eta}{2} + u|\Delta_2|^2 + \frac{\beta}{2}|\Delta_1|^2 & \frac{u}{2}\Delta_2^2 + \frac{\alpha}{2}\Delta_1^2 \\ \frac{\beta}{2}\Delta_1^*\Delta_2^* & \frac{\beta}{2}\Delta_1\Delta_2^* + \alpha\Delta_1^*\Delta_2 & \frac{u}{2}\Delta_2^2 + \frac{\alpha}{2}\Delta_1^2 & \frac{a+\eta}{2} + u|\Delta_2|^2 + \frac{\beta}{2}|\Delta_1|^2 \end{pmatrix} \quad (27)$$

Because we are interested only in the energy gap of the collective modes, and not in their dispersions, we ignore the spatial dependence of the SC gap. The energies of the four collective modes are therefore given by:

$$\omega_i = \sqrt{\frac{\lambda_i}{\gamma_{\text{sc}}}} \quad (28)$$

where λ_i are the eigenvalues of the matrix $\mathbf{\Lambda}$. We first focus in the SC₁ phase, $T_c^* < T < T_c$, in which the equilibrium gap functions $\Delta_{i,0}$ are given by Eqs. (6). Diagonalizing the matrix $\mathbf{\Lambda}$ gives the following eigenvalues:

$$\begin{aligned} \lambda_1 &= 0 \\ \lambda_2 &= -a + \eta \\ \lambda_3 &= \frac{a(u + \alpha - \beta) + \eta(u - \alpha + \beta)}{2u} \\ \lambda_4 &= \frac{a(u - \alpha - \beta) + \eta(u + \alpha + \beta)}{2u} \end{aligned} \quad (29)$$

with the corresponding eigenvectors:

$$\begin{aligned} \mathbf{v}_1^T &= (-1 \ 1 \ 0 \ 0) \\ \mathbf{v}_2^T &= (1 \ 1 \ 0 \ 0) \\ \mathbf{v}_3^T &= (0 \ 0 \ 1 \ -1) \\ \mathbf{v}_4^T &= (0 \ 0 \ 1 \ 1) \end{aligned} \quad (30)$$

Clearly, the two SC components Δ_1 and Δ_2 decouple in this regime. The expressions for the eigenvectors reveal

that the eigenvalue λ_1 corresponds to the phase mode of the condensed SC component. Although in our calculation it vanishes, it becomes a massive mode once the coupling to the electronic density is included (Anderson-Higgs mechanism)^{74–76}. The eigenvalue λ_2 is the amplitude mode of the Δ_1 gap. Although it becomes soft at T_c , since $a_c = \eta$, it does not give rise to a sharp collective mode because at T_c the electronic spectrum is barely gapped, implying that the mode falls into the particle-hole continuum.

The other two eigenvalues correspond to modes of the incipient Δ_2 component, which condenses only at T_c^* . Because it condenses with a relative phase of $\pi/2$ with respect to Δ_1 , λ_3 corresponds to an incipient amplitude mode, whereas λ_4 corresponds to an incipient relative phase mode. Because the latter does not couple directly to the electronic density, it does not become massive below T_c^* . Interestingly, we observe that at T_c^* , which corresponds to:

$$a_* = -\eta \left(\frac{u + \beta - \alpha}{u - \beta + \alpha} \right), \quad (31)$$

the mode λ_3 becomes soft. In this case, because Δ_1 has already been condensed at T_c , the electronic spectrum is gapped, implying that this collective excitation can be a sharp mode in the vicinity of T_c^* . To analyze how these modes evolve below T_c^* , we diagonalize the matrix $\mathbf{\Lambda}$ in the SC₂ phase, $T \leq T_c^*$, in which $\Delta_{i,0}$ is given by Eq. (7). We obtain:

$$\begin{aligned} \lambda_1 &= 0 \\ \lambda_2 &= \frac{-au}{u + \beta - \alpha} + \sqrt{\eta^2 \left(\frac{u + \beta - \alpha}{u - \beta + \alpha} \right) + \frac{a^2(\beta - \alpha)^2}{(u + \beta - \alpha)^2}} \\ \lambda_3 &= \frac{-au}{u + \beta - \alpha} - \sqrt{\eta^2 \left(\frac{u + \beta - \alpha}{u - \beta + \alpha} \right) + \frac{a^2(\beta - \alpha)^2}{(u + \beta - \alpha)^2}} \\ \lambda_4 &= \frac{-2a\alpha}{u + \beta - \alpha} \end{aligned} \quad (32)$$

Although the corresponding eigenvectors are straightforward to obtain, we refrain from writing explicitly their lengthy expressions here. In Fig. 9, we plot the eigenvalues λ_2 , λ_3 , and λ_4 as function of temperature inside the SC state. As discussed above, λ_3 , corresponding to the incipient Δ_2 amplitude mode, vanishes at T_c^* . This opens the interesting possibility of detecting the second SC transition spectroscopically. For instance, Raman scattering in the symmetry channel corresponding to the Δ_2 component (B_{3g}/B_{2g} irreducible representation of the orthorhombic point group) could in principle detect a sharp mode near T_c^* inside the gapped region of the spectrum ($\omega < 2\Delta_1$).

An important issue ignored in the analysis above is the fact that the superconducting state has nodal quasi-particle excitations, which in principle couple to the λ_3

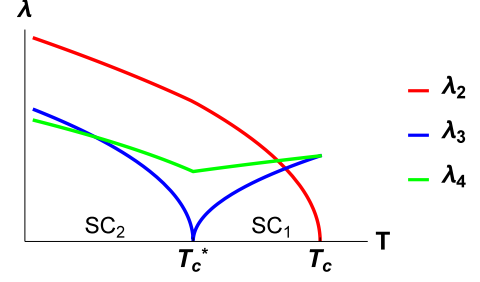


Figure 9. Eigenmodes of the SC state inside the HO phase, as explained in the main text: λ_2 (red), λ_3 (blue), and λ_4 (green). λ_1 , corresponding to the global phase mode, is not shown, since it becomes massive due to the coupling to the electronic density.

mode and can cause damping. To investigate this effect, we compute the one-loop bosonic self-energy diagram containing the coupling of Δ_2 to the electronic states (and particularly to the nodal quasi-particles) at the vicinity of T_c^* , where the λ_3 mode becomes soft (see Fig. 10). At this temperature, the SC gap Δ_1 is fully developed. Therefore, in Nambu space, the electronic Green's function is given by:

$$G(\vec{k}, i\nu_n) = \int \frac{dz}{2\pi} \frac{A(\vec{k}, z)}{i\nu_n - z}, \quad (33)$$

with $\nu_n = (2n + 1)\pi T$ and the spectral function:

$$\begin{aligned} A(\vec{k}, z) &= \frac{\pi}{E_{\vec{k}}} (\delta(z - E_{\vec{k}}) - \delta(z + E_{\vec{k}})) \\ &\times (z\sigma_0 + \xi_{\vec{k}}\sigma_3 - \Delta_1(\vec{k})\sigma_1) \end{aligned} \quad (34)$$

where $E_{\vec{k}} = \sqrt{\xi_{\vec{k}}^2 + \Delta_1^2(\vec{k})}$ is the nodal quasi-particle excitation and σ_i are Pauli matrices in Nambu space. Thus, the bosonic self-energy shown in Fig. 10 becomes:

$$\begin{aligned} \Pi(i\omega_n) &= -T \sum_m \int \frac{d^d k}{(2\pi)^d} \int \frac{dz_1}{2\pi} \int \frac{dz_2}{2\pi} \\ &\times \frac{\pi^2 \text{tr} \left[g(\hat{k})\sigma_2 A(\vec{k}, z_1) g(\hat{k})\sigma_2 A(\vec{k}, z_2) \right]}{E_{\vec{k}}^2 (i\nu_m + i\omega_n - z_1)(i\nu_m - z_2)} \end{aligned} \quad (35)$$

Here we set the external momentum $q = 0$ (since we are only interested in the dynamics) and included the Nambu vertex $g(\hat{k})\sigma_2 = \sin(2\theta)\sin(\phi - \pi/4)\sigma_2$ corresponding to $\Delta_2(\vec{k}) = \Delta_2 g(\hat{k})\sigma_2$. A straightforward calculation gives:

$$\begin{aligned} \Pi(i\omega_n) &= \int \frac{d^d k}{(2\pi)^d} \tanh\left(\frac{\beta E_{\vec{k}}}{2}\right) \\ &\left(\frac{1}{i\omega + 2E_{\vec{k}}} - \frac{1}{i\omega - 2E_{\vec{k}}} \right) g^2(\hat{k}) \end{aligned} \quad (36)$$

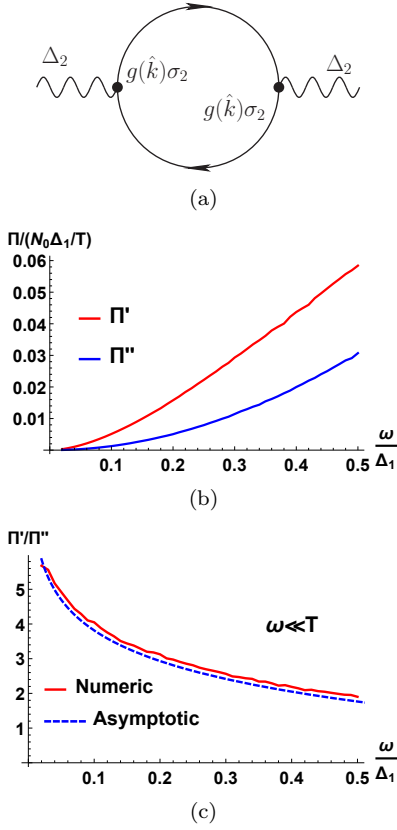


Figure 10. Upper panel: Bosonic SC self-energy (in Nambu space) arising from the coupling between Δ_2 and the quasi-particles near T_c^* . Here $g(\hat{k}) = \sin(2\theta)\sin(\phi - \pi/4)$. Middle panel: the real and imaginary parts of the bosonic self energy when $\omega \ll T$. Lower panel: The ratio between the real and the imaginary parts of the frequency-dependent bosonic self-energy. It is clear that the real part is much smaller than the imaginary part at low frequencies. Moreover, since the imaginary part is proportional to ω^2 and not to ω , the mode is under-damped.

Performing the analytic continuation and subtracting the frequency-independent part, $\Pi(0)$, we obtain the imaginary and real parts of $\delta\Pi(\omega) = \Pi(\omega) - \Pi(0)$ (hereafter we consider $\omega > 0$):

$$\begin{aligned}\delta\Pi''(\omega) &= \pi \tanh\left(\frac{\beta\omega}{4}\right) \int \frac{d^d k}{(2\pi)^d} \delta(\omega - 2E_{\vec{k}}) g^2(\hat{k}) \\ \delta\Pi'(\omega) &= \int \frac{d^d k}{(2\pi)^d} \tanh\left(\frac{\beta E_{\vec{k}}}{2}\right) \frac{\omega^2 g^2(\hat{k})}{E_{\vec{k}}(4E_{\vec{k}}^2 - \omega^2)}\end{aligned}\quad (37)$$

In the limit $\omega \ll \Delta_1, T$, we find the low-energy asymptotic behaviors of the bosonic self-energy:

$$\begin{aligned}\delta\Pi''(\omega) &\approx \frac{\pi N_0}{24} \frac{\omega^2}{T\Delta_1} \\ \delta\Pi'(\omega) &\approx \frac{N_0}{6} \frac{\omega^2}{T\Delta_1} \log\left(\frac{2\Delta_1}{\omega}\right)\end{aligned}\quad (38)$$

Thus, at low enough frequencies, not only does the imaginary part varies quadratically with the frequency, but also the real part is much larger than the imaginary part. Consequently, the λ_3 mode can still be sharp near T_c^* despite the damping introduced by its coupling to the nodal quasi-particles. To confirm these analytical results, in Fig. 10, we plot the behavior of $\delta\Pi''(\omega)$ and $\delta\Pi'(\omega)$ evaluated numerically from Eqs. (37), evidencing the sub-leading character of the imaginary part.

V. CONCLUDING REMARKS

In summary, we have investigated the impact of the tetragonal symmetry breaking promoted by the HO phase in the low-temperature chiral SC state of URu₂Si₂. Besides the anticipated splitting of the SC transition into two, the two resulting SC phases display very different low-energy behaviors. In particular, the nodal quasi-particle density of states of the higher-temperature SC phase acquires an anomalous logarithmic dependence due to the crossing of two nodal lines. Although absent in the lower-temperature SC phase at low energies, this log-behavior can in principle still be manifested for intermediate energy ranges as a crossover effect. We have also shown the softening of one of the amplitude SC modes near the second SC transition, providing yet another signature of the interplay between tetragonal symmetry breaking and SC. Finally, we showed that the current angle-resolved specific-heat data is qualitatively consistent with either a tetragonal chiral state or an orthorhombic chiral state. We propose additional measurements in the presence of uniaxial strain to unambiguously distinguish the two scenarios.

It is important to critically analyze our results in face of recent data on the SC state of URu₂Si₂. First, our phenomenological model relies on the applicability of a Ginzburg-Landau approach. Although this seems to be the case in URu₂Si₂ given the behavior of the thermodynamic quantities across T_c , large SC fluctuations have been recently proposed in Ref.⁸⁰. As for the existence of two SC transitions, the temperature dependence of H_{c1} has been interpreted as indirect evidence for one SC transition at $T_c \approx 1.5$ K followed by a second one at $T_c^* \approx 1.2$ K³⁵. In contrast, recent Kerr data seem to be consistent with time-reversal symmetry being broken at T_c ⁴⁹. If this is indeed the case, it would imply that the tetragonal symmetry breaking at the HO transition is inconsequential for SC. On the other hand, the same data set reveals an anomalous Kerr signal well below T_c , at $T \approx 1$ K. This anomaly, combined with a “background” Kerr signal that onsets at high temperatures, indicates that at least for now one cannot rule out the possibility of two SC transitions in URu₂Si₂. As pointed out in Ref. [49], additional data are needed to settle this issue. An interesting possibility would be to perform Kerr measurements in strained samples. Due to the dependence of T_c^* on the strain field, such a measurement would elucidate

whether the anomalous Kerr signal could be a manifestation of a second SC transition.

Our phenomenological results offer robust benchmarks that can be employed to study the interplay between the tetragonal symmetry breaking promoted by the HO state and the time-reversal symmetry-breaking promoted by the SC state in URu₂Si₂. With appropriate modifica-

tions, our model should also be relevant to other systems in which chiral SC states have been proposed, such as the ruthenates⁷⁸ and doped graphene⁷⁹.

We thank A. Chubukov, I. Fisher, R. Flint, A. Kamenev, A. Maharaj, Y. Matsuda, and S. Raghu for fruitful discussions. This work was supported by the U.S. Department of Energy, Office of Science, Basic Energy Sciences, under award number de-sc0012336.

-
- ¹ T. M. Palstra, A. A. Menovsky, J. van den Berg, A. J. Dirkmaat, P. H. Kes, G. J. Nieuwenhuys, and J. A. Mydosh, *Phys. Rev. Lett.* **55**, 2727 (1985).
 - ² M. B. Maple, J. W. Chen, Y. Dalichaouch, T. Kohara, C. Rossel, M. S. Torikachvili, M. W. McElfresh, and J. D. Thompson, *Phys. Rev. Lett.* **56**, 185 (1987).
 - ³ W. Schlitz, J. Baumann, B. Pollit, U. Rauchschwalbe, H. M. Mayer, U. Ahlheim, and C. D. Bredl, *Z. Phys. B* **62**, 171 (1986).
 - ⁴ G. J. Nieuwenhuys, *Phys. Rev. B* **35**, 5260 (1987).
 - ⁵ V. Barzykin and L. P. Gor'kov, *Phys. Rev. Lett.* **74**, 4301 (1995).
 - ⁶ H. Harima, K. Miyake, and J. Flouquet, *J. Phys. Soc. Jpn.* **79**, 033705 (2010).
 - ⁷ F. J. Ohkawa and H. Shimizu, *J. Phys. Condens. Matter* **11**, 519 (1999).
 - ⁸ K. Hanzawa and N. Watanabe, *J. Phys. Condens. Matter* **17**, 419 (2005).
 - ⁹ K. Hanzawa, *J. Phys. Condens. Matter* **19**, 072202 (2005).
 - ¹⁰ K. Haule and G. Kotliar, *Nature Phys.* **5**, 796 (2009).
 - ¹¹ F. Cricchio, F. Bultmark, O. Grånäs, and Lars Nordström, *Phys. Rev. Lett.* **103**, 107202 (2009).
 - ¹² H. Kusunose and H. Harima, *J. Phys. Soc. Jpn.* **80**, 084702 (2011).
 - ¹³ L. P. Gor'kov, *Europhys. Lett.* **16**, 301 (1991).
 - ¹⁴ L. P. Gor'kov and A. Sokol, *Phys. Rev. Lett.* **69**, 2586 (1992).
 - ¹⁵ A. P. Ramirez, P. Coleman, P. Chandra, E. Brück, A. A. Menovsky, Z. Fisk, and E. Bucher, *Phys. Rev. Lett.* **68**, 2680 (1992).
 - ¹⁶ P. Santini and G. Amoretti, *Phys. Rev. Lett.* **73**, 1027 (1994).
 - ¹⁷ V. P. Mineev and M. E. Zhitomirsky, *Phys. Rev. B* **72**, 014432 (2005).
 - ¹⁸ H. Ikeda and Y. Ohashi, *Phys. Rev. Lett.* **81**, 3723 (1998).
 - ¹⁹ P. Kotetes and G. Varelogiannis, *Phys. Rev. Lett.* **104**, 106404 (2010).
 - ²⁰ P. Kotetes, A. Aperis, and G. Varelogiannis, *Philos. Mag.* **10.1080/14786435.2014.909614** (2014).
 - ²¹ C. M. Varma and L. Zhu, *Phys. Rev. Lett.* **96**, 036405 (2006).
 - ²² A.V. Silhanek, N. Harrison, C.D. Batista, M. Jaimea, A. Lacerta, H. Amitsuka, and J.A. Mydosh, *Physica B* **378**, 373 (2006).
 - ²³ P. Chandra, P. Coleman, J. A. Mydosh and V. Tripathi, *Nature* **417**, 831 (2002).
 - ²⁴ V. Tripathi, P. Chandra, and P. Coleman, *J. Phys. Condens. Matter* **17**, 5285 (2005).
 - ²⁵ P. Chandra, P. Coleman, and R. Flint, *Nature* **493**, 621 (2013).
 - ²⁶ P. Fazekas, A. Kiss, and K. Radnózi, *Prog. Theor. Phys. Suppl.* **160**, 114 (2005).
 - ²⁷ H. Ikeda, M.-T. Suzuki, R. Arita, T. Takimoto, T. Shibauchi, and Y. Matsuda, *Nat. Phys.* **8**, 528 (2012).
 - ²⁸ Y. Dubi and A.V. Balatsky, *Phys. Rev. Lett.* **106**, 086401 (2011).
 - ²⁹ S. Fujimoto, *Phys. Rev. Lett.* **106**, 196407 (2011).
 - ³⁰ C. Pépin, M. R. Norman, S. Burdin, and A. Ferraz, *Phys. Rev. Lett.* **106**, 106601 (2011).
 - ³¹ J.G. Rau and H.Y. Kee, *Phys. Rev. B* **85**, 245112 (2012).
 - ³² S. Elgazzar, J. Ruzs, M. Amft, P. M. Oppeneer, and J. A. Mydosh, *Nat. Mater.* **8**, 337 (2009).
 - ³³ T. Das, *Phys. Rev. B* **89**, 045135 (2014).
 - ³⁴ R. Okazaki, T. Shibauchi, H. J. Shi, Y. Haga, T. D. Matsuda, E. Yamamoto, Y. Onuki, H. Ikeda, Y. Matsuda, *Science* **331**, 439 (2011).
 - ³⁵ T. Shibauchi and Y. Matsuda, *Physica C* **481**, 299 (2012).
 - ³⁶ S. Tonegawa, S. Kasahara, T. Fukuda, K. Sugimoto, N. Yasuda, Y. Tsuruhara, D. Watanabe, Y. Mizukami, Y. Haga, T. D. Matsuda, E. Yamamoto, Y. Onuki, H. Ikeda, Y. Matsuda, and T. Shibauchi, *Nat. Commun.* **5**, 4188 (2014).
 - ³⁷ S. C. Riggs, M. C. Shapiro, A. V. Maharaj, S. Raghu, E. D. Bauer, R. E. Baumbach, P. Giraldo-Gallo, M. Wartenbe, and I. R. Fisher, *Nat. Commun.* **6**, 6425 (2015).
 - ³⁸ J. Buhot, M.-A. Méasson, Y. Gallais, M. Cazayous, G. Lapertot, D. Aoki, and A. Sacuto, *Phys. Rev. Lett.* **113**, 266405 (2014).
 - ³⁹ H.-H. Kung, R. E. Baumbach, E. D. Bauer, V. K. Thorsmølle, W.-L. Zhang, K. Haule, J. A. Mydosh, and G. Blumberg, *Science* **347**, 1339 (2015).
 - ⁴⁰ E. Hassinger, G. Knebel, T. D. Matsuda, D. Aoki, V. Taufour, and J. Flouquet, *Phys. Rev. Lett.* **105**, 216409 (2010).
 - ⁴¹ E. Ressouche et al., *Phys. Rev. Lett.* **109**, 067202 (2012).
 - ⁴² A. V. Balatsky, A. Chantis, Hari P. Dahal, David Parker, and J. X. Zhu, *Phys. Rev. B* **79**, 214413 (2009).
 - ⁴³ C.-H. Hsu and S. Chakravarty, *Phys. Rev. B* **87**, 085114 (2013); *Phys. Rev. B* **90**, 134507 (2014).
 - ⁴⁴ S. Uemura, G. Motoyama, Y. Oda, T. Nishioka, and N. K. Sato, *J. Phys. Soc. Japan* **74**, 2667 (2005).
 - ⁴⁵ J. R. Jeffries, N. P. Butch, B. T. Yukich, and M. B. Maple, *J. Phys.: Condens. Matter* **20**, 095225 (2008).
 - ⁴⁶ K. Yano, T. Sakakibara, T. Tayama, M. Yokoyama, H. Amitsuka, Y. Homma, P. Miranović, M. Ichioka, Y. Tsutsumi, and K. Machida, *Phys. Rev. Lett.* **100**, 017004 (2008).
 - ⁴⁷ Y. Kasahara, H. Shishido, T. Shibauchi, Y. Haga, T. D. Matsuda, Y. Onuki, and Y. Matsuda, *New J. Phys.* **11**, 055061 (2009).
 - ⁴⁸ G. Li, Q. Zhang, D. Rhodes, B. Zeng, P. Goswami, R. E. Baumbach, P. H. Tobash, F. Ronning, J. D. Thompson, E. D. Bauer, and L. Balicas, *Phys. Rev. B* **88**, 134517 (2013).

- ⁴⁹ E. R. Schemm, R. E. Baumbach, P. H. Tobash, F. Ronning, E. D. Bauer, and A. Kapitulnik, Phys. Rev. B **91**, 140506 (2015).
- ⁵⁰ T. Shibauchi, H. Ikeda, and Y. Matsuda, Philo. Mag. **94**, 3747 (2014).
- ⁵¹ G. E. Volovik, JETP Lett. **58**, 469 (1993).
- ⁵² M. Sigrist, R. Joynt, and T. M. Rice, Phys. Rev. B **36**, 5186 (1987).
- ⁵³ S. Takamatsu and Y. Yanase, Phys. Rev. B **91**, 054504 (2015).
- ⁵⁴ I. R. Fisher, L. Degiorgi, and Z. X. Shen, Rep. Prog. Phys. **74**, 124506 (2011).
- ⁵⁵ R. M. Fernandes, A. V. Chubukov, and J. Schmalian, Nature Phys. **10**, 97 (2014).
- ⁵⁶ P. M. Oppeneer, J. Rusz, S. Elgazzar, M.-T. Suzuki, T. Durakiewicz, and J. A. Mydosh, Phys. Rev. B **82**, 205103 (2010).
- ⁵⁷ H. Ohkuni, Y. Inada, Y. Tokiwa, K. Sakurai, R. Settai, T. Honma, Y. Haga, E. Yamamoto, Y. Onukia, H. Yamagami, S. Takahashi, and T. Yanagisawa, Philos. Mag. B **79** 1045 (1999).
- ⁵⁸ H. Shishido, K. Hashimoto, T. Shibauchi, T. Sasaki, H. Oizumi, N. Kobayashi, T. Takamasu, K. Takehana, Y. Imanaka, T. D. Matsuda, Y. Haga, Y. Onuki, and Y. Matsuda, Phys. Rev. Lett. **102** 156403 (2009).
- ⁵⁹ M. M. Altarawneh, N. Harrison, S. E. Sebastian, L. Balicas, P. H. Tobash, J. D. Thompson, F. Ronning, and E. D. Bauer, Phys. Rev. Lett. **106** 146403 (2011).
- ⁶⁰ S. Tonegawa, K. Hashimoto, K. Ikada, Y. Tsuruhara, Y.-H. Lin, H. Shishido, Y. Haga, T. D. Matsuda, E. Yamamoto, Y. Onuki, H. Ikeda, Y. Matsuda, and T. Shibauchi, Phys. Rev. B **88**, 245131 (2013).
- ⁶¹ R. M. Fernandes and J. Schmalian, Phys. Rev. B **84**, 012505 (2011).
- ⁶² V. Stanev, B. S. Alexandrov, P. Nikolic, and Z. Tesanovic, Phys. Rev. B **84**, 014505 (2011).
- ⁶³ B. Mazidian, J. Quintanilla, A. D. Hillier, and J. F. Annett, Phys. Rev. B **88**, 224504 (2013).
- ⁶⁴ J. Kang, A. F. Kemper, and R. M. Fernandes, Phys. Rev. Lett. **113**, 217001 (2014).
- ⁶⁵ I. Vekhter, P. J. Hirschfeld, and E. J. Nicol, Phys. Rev. B **64**, 064513 (2001).
- ⁶⁶ A. Vorontsov and I. Vekhter, Phys. Rev. B **75**, 224501 (2007).
- ⁶⁷ C. Mirri, A. Dusza, S. Bastelberger, M. Chinotti, J.-H. Chu, H.-H. Kuo, I. R. Fisher, and L. Degiorgi, arXiv:1504.06829.
- ⁶⁸ A. Larkin, A. Varlamov, *Theory of fluctuations in superconductors*, Oxford University Press (2005).
- ⁶⁹ J. Carlström, J. Garaud, and E. Babaev, Phys. Rev. B **84**, 134518 (2011).
- ⁷⁰ V. Stanev, Phys. Rev. B **85**, 174520 (2012).
- ⁷¹ S. Maiti, and A. V. Chubukov, Phys. Rev. B **87**, 144511 (2013).
- ⁷² A. Bardasis and J. R. Schrieffer, Phys. Rev. **121**, 1050 (1961).
- ⁷³ D. Pekker and C. M. Varma, Annu. Rev. Condens. Matter Phys. **6** (2015).
- ⁷⁴ P. W. Anderson, Phys. Rev. **110**, 827 (1958).
- ⁷⁵ P. B. Littlewood and C. M. Varma, Phys. Rev. B **26**, 4883 (1982).
- ⁷⁶ R. Cöte, A. Griffin, Phys. Rev. B **48**, 10404(1993).
- ⁷⁷ A. J. Leggett, Prog. of Theor. Phys. **36**, 901 (1966).
- ⁷⁸ C. W. Hicks, D. O. Brodsky, E. A. Yelland, A. S. Gibbs, J. A. N. Bruin, K. Nishimura, S. Yonezawa, Y. Maeno, and A.P. Mackenzie, Science **344**, 283 (2014).
- ⁷⁹ R. Nandkishore, L. Levitov, and A. V. Chubukov, Nature Phys. **8**, 158 (2012).
- ⁸⁰ T. Yamashita, Y. Shimoyama, Y. Haga, T. D. Matsuda, E. Yamamoto, Y. Onuki, H. Sumiyoshi, S. Fujimoto, A. Levchenko, T. Shibauchi, and Y. Matsuda, Nat. Phys. **11**, 17 (2015).